Deep Sea Research Part I: Oceanographic Research Papers
November 2009, Volume 56, Issue 11, Pages 2026-2040
http://dx.doi.org/10.1016/j.dsr.2009.06.006

Distribution and spatial variation of hydrothermal faunal assemblages at Lucky Strike (Mid-Atlantic Ridge) revealed by high-resolution video image analysis

Daphne Cuvelier[a], Jozée Sarrazin[b], Ana Colaço[a], Jon Copley[c], Daniel Desbruyères[b], Adrian G. Glover[d], Paul Tyler[c] and Ricardo Serrão Santos[a]

[a] IMAR/Department of Oceanography and Fisheries, University of the Azores, Cais de Santa Cruz, 9901-862 Horta, Portugal
[b] Institut Français de Recherche pour l'Exploitation de la Mer (Ifremer), Centre de Brest, Département Études des Ecosystèmes Profonds, Laboratoire Environnement Profond, BP 70, 29280 Plouzané, France
[c] National Oceanography Centre, Southampton, University of Southampton Waterfront Campus, European Way, Southampton SO14 3ZH, UK
[d] Zoology Department, The Natural History Museum, Cromwell Rd, London SW7 5BD, UK

*: Corresponding author : D. Cuvelier, Tel.: +351 292 200 400; fax: +351 292 20 0411, email address : daphne.cuvelier@gmail.com
Co-authors email addresses (respectively):
Jozee.Sarrazin@ifremer.fr
acolaco@uac.pt
itc@noc.soton.ac.uk
Daniel.Desbruyeres@ifremer.fr
a.glover@nhm.ac.uk
pat8@noc.soton.ac.uk
ricardo@uac.pt

Abstract:

Whilst the fauna inhabiting hydrothermal vent structures in the Atlantic Ocean is reasonably well known, less is understood about the spatial distributions of the fauna in relation to abiotic and biotic factors. In this study, a major active hydrothermal edifice (Eiffel Tower, at 1690 m depth) on the Lucky Strike vent field (Mid-Atlantic Ridge (MAR)) was investigated. Video transects were carried out by ROV *Victor 6000* and complete image coverage was acquired. Four distinct assemblages, ranging from dense larger-sized *Bathymodiolus* mussel beds to smaller-sized mussel clumps and alvinocaridid shrimps, and two types of substrata were defined based on high definition photographs and video imagery. To evaluate spatial variation, faunal distribution was mapped in three dimensions. A high degree of patchiness characterizes this 11 m high sulfide structure. The differences observed in assemblage and substratum distribution were related to habitat characteristics (fluid exits, depth and structure orientation). Gradients in community structure were observed, which coincided with an increasing distance from the fluid exits. A biological zonation model for the Eiffel Tower edifice was created in which faunal composition and distribution can be visually explained by the presence/absence of fluid exits.

Keywords: Community structure; Spatial distribution; Faunal assemblages; Video analysis; Lucky Strike; Hydrothermal vent; Mid-Atlantic Ridge; Vent ecology

1. INTRODUCTION

Two decades of research on deep-sea hydrothermal vents in the Atlantic Ocean have led to a reasonably good knowledge of the mega-and macro-fauna inhabiting these chemosynthetic habitats. Rather less is known about the community structure and the spatial and temporal distributions of the fauna in relation to abiotic and biotic factors. In particular, small-scale and detailed spatial distribution studies for the Atlantic hydrothermal vents have been scarce. On the other hand, large-scale variations between Atlantic vent fields, have already been investigated (Desbruyères et al., 2000, 2001).

The most important structuring factor for the composition, distribution and dynamics of deep-sea hydrothermal vent assemblages appears to be the high spatial variability of biotic and abiotic factors related to hydrothermal vent activity and more specifically, the chemical composition and flow intensity of the vent fluids (Hessler et al., 1988; Tunnicliffe, 1991; Sarrazin et al., 1997; Shank et al., 1998; Desbruyères et al., 2001; Luther et al., 2001; Govenar et al., 2005). Consequently, alteration of fluid composition or cessation in fluid flow causes small-scale disturbances on short time-scales and can initiate significant faunal changes (Hessler et al., 1985, 1988; Fustec et al., 1987; Tunnicliffe, 1991; Sarrazin et al., 1997; Shank et al., 1998). Biological interactions are also thought to affect the hydrothermal vent community composition (Fustec et al., 1987; Hessler et al., 1988; Tunnicliffe, 1991; Johnson et al., 1994; Shank et al., 1998; Sarrazin et al., 1999; Mullineaux et al., 2003; Govenar et al.; 2005). Typical examples of biological interactions are predation and competition based, for instance, on trophic (e.g. access to hydrogen sulfide or other resources) and topographic (optimal positioning on the structure or limitation in available space) grounds (Hessler et al., 1985; Fustec et al., 1987; Comtet and Desbruyères, 1998). Food partitioning is likely to play a significant role (Levesque et al., 2006; Limen and Juniper, 2006).

For the Pacific Ocean, spatial distribution and high degrees of patchiness and

heterogeneity at hydrothermal vents have been described by many authors (e.g. Jollivet, 1993; Sarrazin et al., 1997; Tsurumi and Tunnicliffe, 2001, 2003; Govenar et al., 2005); these observations are quite often based on imagery data (e.g. Hessler et al., 1985, 1988; Chevaldonné and Jollivet, 1993; Jollivet, 1993; Grehan and Juniper, 1996; Sarrazin et al., 1997). To date, only a few studies have investigated spatial variation in fauna coverage through video imagery in the Atlantic. These studies took place at Broken Spur (3090m depth, Copley et al., 1997), Menez Gwen (850m depth, Colaço et al., 1998) and TAG (3650m depth, Copley et al., 2007).

The present study assesses spatial variation and distribution patterns of faunal assemblages of a large sulfide edifice located on the Mid-Atlantic Ridge (MAR). A continuous overview of Eiffel Tower, Lucky Strike vent field, is provided, including flow features, community composition and the scale of the geological structural features observed. The overall aim was to test the following hypothesis: the proximity to sources of visible fluid flow strongly influences faunal distribution, regardless of the orientation of the edifice. Using a new faunal mapping technique and high-resolution imagery, we aim to provide the first insights into small-scale heterogeneity and zonation patterns on a MAR vent edifice. This up-to-date approach will serve as a reference basis for future studies of temporal trends at dynamic and extreme deep-sea environments such as hydrothermal vents.

2. MATERIAL AND METHODS

2.1. Study site

Lucky Strike vent field (37 °17.5'N, 32° 16’W) was discovered serendipitously in 1992, and has been visually observed since 1993. It is situated in the Azores Triple Junction area at a mean depth of 1700m (Fig. 1a). It is a basalt-hosted site (Langmuir et al., 1997 ; Fouquet et al., 1998 ; Desbruyères et al., 2000), consisting of a large lava lake (ca 300m

diameter) surrounded by numerous active vents located mainly in the north-western and south-eastern zones (Charlou et al., 2000; Humphris et al., 2002; Ondréas et al., 2009) (Fig. 1b). Eiffel Tower is a well-defined hydrothermal edifice and one of the most active at Lucky Strike (Fig. 1c), located in the south-eastern region of the vent field. Slabs are present in this area with cracks from which vent fluids originate (Langmuir et al., 1997; Ondréas et al., 1997, 2009). This irregular edifice hosts some intense black smokers (up to 324°C), active flanges and diffusion zones (<200°C), with shimmering water seeping through (Langmuir et al., 1997; Sarradin et al., 1999; Charlou et al., 2000). The fauna of Eiffel Tower is considered to be representative for the entire vent field (Desbruyères et al., 2001). Like other active hydrothermal structures at shallower depths in the Atlantic Ocean, it is covered with dense mussel beds of the mytilid *Bathymodiolus azoricus* (Van Dover, 1995; Langmuir et al., 1997; Comtet and Desbruyères, 1998; Desbruyères et al., 2000, 2001).

2.2. Image acquisition

During six (out of eleven) dives to the Eiffel Tower edifice (MoMARETO cruise 2006) video transects were carried out by the ROV Victor 6000 which was equipped with a 3-CCD camera, 2 piloting cameras and 5 additional colour cameras. A total of approximately 10 hours of video transects were dedicated to acquiring complete imagery coverage of this well-defined edifice. Two types of video transects were carried out. (1) Vertical video transects were executed from bottom to top and started at a distance of 4 to 5m from the structure, to allow reconstruction of the entire edifice, heading North, East, South, West and their intermediates (see Fig. 1d for terminology used to identify the different sides). (2) Transects were then repeated at a distance of 1m from the edifice. For each side the same heading was maintained and the pan and tilt of the principal camera was set to zero. Zoom levels were kept constant (wide open) during the video sampling, in order to generate similarly scaled and comparable

137 images. Video transects were collected in colour imagery, which allowed a visual study of the
138 assemblages and their distributional patterns. Screen-stills from video imagery had a resolution
139 of 696 x 576 pixels. High definition photographs were taken with a digital still camera (Sony,
140 Cybershot), which was mounted above the principal camera of the ROV and had a resolution
141 of 2048 x 1536 pixels.
142
143 **2.3. Video Analysis**
144 Faunal assemblages and substrata were identified based on high definition
145 photographs and video images (Fig. 2 and Table 1). Observations and identifications from on-
146 screen individuals were ground-truthed with samples taken during the same cruise and with
147 historical sample lists present in the BIOCEAN database (©Ifremer, Fabri et al., 2006). For
148 each assemblage, mussels were measured to confirm the observed difference between larger-
149 and smaller-sized individuals in order to allow a better distinction to be made between
150 assemblage types.
151 Screen stills were taken from video transects with 'Adelie video' (version 1.8, ©Ifremer
152 2005) and were used to reconstruct the hydrothermal structure through mosaicing. Mosaics per
153 edifice side and for zoomed-in regions were created manually in Adobe Photoshop Elements
154 2.2©; pixel lengths were measured and images adjusted one to another and superimposed. The
155 mosaics were used as a template to map the different types of fluid exits (black smokers, active
156 flanges and zones of diffusion) as well as the different assemblages. Visually recognizable
157 geological features on the edifice were used as reference points to localize emissions or
158 assemblages. Vertical transects were studied with different viewing angles (intermediate
159 headings), to make sure no detail was missed and to minimize the distortion effects of
160 protruding rocks, relief and uneven surfaces. Contours were drawn and video transects were
161 watched repeatedly in order to map the fluid exits and the assemblages on the mosaic templates

using colour coding, so they could be digitized. Visually interpretable maps were created for each side of the tower and the periphery. Sampling instruments present on the structure or visible parts of the ROV, when in the same focal plane, were used to scale the mosaics. The proximity (distance and direction) of the assemblages and substrata to fluid exits was measured, as well as the mean patch size for all assemblages and substrata. Patterns and gradients in assemblage distribution were analysed. Systematic transfer patterns between the different neighbouring assemblages were investigated. Counts were made of the number of times that a patch of assemblage X was bordered by a patch of another type of assemblage (Y). A patch was defined as an enclosed surface occupied by a certain type of assemblage or an uncolonised surface (substratum).

All image analysis operations, i.e. length/distance measurements and surface calculations, are pixel based and were carried out by the Image analysing program IP Lab Spectrum®. Each patch surface was measured 3 times to reduce error from online tracing (in analogy with Sarrazin et al., 1997).

2.4. Statistics

Statistical analyses of percentage cover and distances were carried out both in R (version 2.7, Multicore team 2008) and in Statistica 6 (StatSoft Inc 2001). Ordinations in R were performed with the Vegan package (Oksanen et al., 2008). Data used in the multivariate analyses were linearly distributed hence PCA (Principal Component Analysis) and RDA (Redundancy Analysis) were used. For the cluster analysis Ward's method was used for Euclidean distances. The Friedman's test is the non-parametric equivalent of a two-way ANOVA used to compare multiple dependent samples, in this case the size of the patches between the sides**.** Factorial ANOVA's and the Tukey HSD post-hoc test were used to compare minimum and maximum distance to a fluid exit between the different assemblages

187 and substrata. Correlations (Spearman Rank) were calculated between the number of visible
188 black smokers, flanges and diffusion zones and between the assemblages and substrata,
189 between all sides (n=7, degrees of freedom=5).
190
191 # 3. RESULTS
192 ## 3.1. Eiffel Tower morphology and activity
193 The Eiffel Tower edifice extends 11m in height and at most 20m in width and was
194 divided into two parts, a 'tower' structure consisting of the upper 8m (summit at 1681m of
195 depth) and a 'periphery' including the lower 3-4m until the seafloor is reached at a depth of
196 1692m. The overall Eiffel Tower morphology did not change drastically during the
197 MoMARETO cruise. However, several structural differences were noted between the dives;
198 black chimneys of freshly precipitated minerals grew more than 0.5m per night (structures
199 were sampled for certain experiments and grew back after one night, sometimes overgrowing
200 sampling devices, D. Cuvelier, pers. obs.).
201 The number of black smokers and the number of diffusion zones were positively
202 correlated (R^2=0.944, p=0.001): their numbers increased proportionally one to another. Flanges
203 were not correlated with either black smokers or diffusion zones. The hydrothermal activity
204 spread out towards the periphery since highly-active black smoker chimneys were observed at
205 the base of the edifice, on the southern periphery and on the structure between North and West
206 sides (Fig. 1d). No activity was observed, however, on the eastern periphery, and no associated
207 life was present. Therefore this part of the structure was not included in the analyses.
208
209 ## 3.2. Faunal composition of the Eiffel Tower edifice
210 The taxonomic composition of the vent fauna inhabiting Eiffel Tower was determined
211 through the use of both video imagery, still photography and past and ongoing faunal

sampling (Table 1). The resolution of video precludes the identification of smaller organisms; however, larger macro- and mega-fauna could be identified in most cases to species level. The main species associated with the vent were the mussel *Bathymodiolus azoricus,* and three species of alvinocaridid shrimp, namely *Mirocaris fortunata*, *Chorocaris chacei* and *Alvinocaris markensis*. Bytograeid crabs (*Segonzacia mesatlantica*) and many other less conspicuous species lived in association with these mussel beds (Desbruyères et al., 2006). *Bathymodiolus azoricus* was the most abundant component of 2 out of the 4 assemblages, creating a microhabitat for other accompanying organisms (Table 1). Of the three species of shrimps present on Eiffel Tower, *A. markensis* was the most solitary, followed by *C. chacei,* which lived in small groups of low numbers. The smallest species, *M. fortunata*, was the most gregarious and abundant over the entire edifice; it co-occurred with *C. chacei*. *Alvinocaris markensis* was occasionally seen on top of or in between the larger-sized mussel beds. The mobility of all these alvinocaridids decreased when close by or in the actual warm water flow. If present in warm shimmering water, they were almost immobile, in contrast to the rapid movements when moving between and over mussels.

Segonzacia mesatlantica (Bythograeidae, Decapoda) is a typical vent species on the MAR and occurred anywhere on the edifice, in shimmering water, crawling in between and over mussel beds and clumps, hiding underneath them or crossing bare surfaces, etc. Sometimes they were observed traversing the microbial mats.

Towards the base and periphery of the edifice, ophiuroids were observed. Although difficult to identify from the video imagery, the species is most likely to be *Ophioctenella acies* (P. Tyler, pers. obs.), which seems to show an affinity for *Bathymodiolus* beds (Desbruyères et al., 2006). Gastropod grazers (Lepetodrilidae and other families) were observed on mussel shells and bare rocks, also mostly towards the base of the structure (Table 1). A diverse associated ichthyofauna was also associated with the edifice. These fish were

observed making regular predatory incursions (e.g. *Hydrolagus pallidus* (Chimaeridae), *Synaphobranchus sp.* (Synaphobranchidae), *Coryphaenoides armatus* (Macrouridae)) or living in cracks and crevices of the chimney (*Gaidropsarus* sp. (Moridae)). *Cataetyx laticeps* (Bythitidae) was observed almost every time a video transect was executed, lying immobile at the base of the edifice. This species often occurred in pairs.

3.3. Assemblages

To understand small-scale heterogeneity on the vent edifice, we identified and quantified distinct assemblages defined by the presence or absence of key taxa, their size and their coverage. Distinct substratum types were also identified based on the type of mineralization and, in some cases, microbial cover.

Four distinct assemblages and two substratum types were identified (Fig. 2) of which two assemblages and one substratum had two subordinate forms ("a" without and "b" with visible microbial coverage). Assemblage 1 consisted of dense mussel beds (the mussels are of the larger size class, in general >4cm) often with shrimps crawling over and between them. Some limpets were present on the mussel shells. Assemblage 1 mussel beds were found in the neighbourhood of fluid exits, but they were never present in the hot water flow (Fig. 2a). Assemblage 2 comprised clusters of mussels (clumps) with bare surface visible between them (Fig. 2b and c, respectively without and with microbial cover). In this case, the mussels were almost always less than 4cm in length. Alvinocaridid shrimps were observed, but they were not as abundant as in Assemblage 1. Uncovered surfaces colonised by shrimps constituted Assemblage 3 (Fig. 2d). *Mirocaris fortunata* was always present, quite often accompanied by less numerous *Chorocaris chacei*. Assemblage 3 was found mostly in the direct proximity of the warm water flow from the fluid exits, or within the flow itself. Assemblage 4 was characterized by dispersed small mussels and/or new recruits on bare surface (the latter

prevails). Assemblage 4a had no microbial cover (Fig. 2e), and scattered hydroids and limpets were present next to the newly recruited mussels. Assemblages 4b, with microbial cover, lacked hydroids, but limpets were encountered (Fig. 2e). Assemblage 4 was often situated at the base of the tower (or in the periphery), often with large dead mussel shells below the base, possibly fallen from the wall of the structure.

In addition to the assemblages, two substratum types were detected. The main visual difference between these two substrata is their colour. Substratum 1a was a bare, brownish to reddish uncolonised surface (Fig. 2f) while Substratum 1b represented a similar surface covered by whitish filamentous bacteria (Fig. 2g). Occasionally decapods were present. Substratum 2 had a white-mottled surface due to anhydrite deposits; patchy microbial mats were sometimes also present (Fig. 2h). This substratum often occurred in very hot regions with the presence of black smokers, shimmering water and/or diffusion. Black chimneys composed of freshly deposited minerals were never colonised permanently, but were sometimes visited by shrimps and crabs from surrounding patches (Table 1).

3.4. Spatial distribution and size of the assemblages

The visually interpretable maps showing the spatial assemblage and substratum distribution are presented in Fig. 3. Assemblages 4a and 4b were considered as 'uncolonised' surface because bare surfaces largely predominate. Counts (number m^{-2}) of visible active features (black smokers, flanges and diffusion zones) showed variations between structure sides as well (Table 2).

The East and South sides, which were the least strongly colonised (Fig. 3e and g), had quite large proportions of Assemblages 1 and 3 and Substratum 2 (Fig. 3h) compared to the other sides, and also showed the highest level of visible hydrothermal activity (Table 2). Conversely, the North and West sides, which were colonised most intensively (Fig. 3a and d),

were dominated by Assemblages 2a and 2b (Fig. 3h) and showed the lowest level of activity (Table 2). The peripheral zones (Fig. 3b, c and f) demonstrated similar trends of high activity, low degree of colonisation, and vice versa. The southern peripheral zone was the least colonised (Fig. 3f) and dominated by Assemblages 4a and 4b (Fig. 3h). It showed a large amount of activity, but this was limited to a few highly-active high-temperature exits (Table 2). The western periphery was the most active, with the highest number of active venting structures in proportion to its surface (Table 2), but the fluid flow was visibly less intense than that on the South side.

The number of patches (see description above in '2.3. Video Analysis') occupied by the different assemblages differed between the sides. Assemblage 2a had always the highest number of patches, regardless of the side it occurred on. However, the total number of patches did not necessarily reflect the total surface covered by an assemblage since the sizes of the patches was variable. For example, while Assemblage 2a had 46 patches on the North side, the surface it covered was estimated to be 4.50 m^2 on this side of the edifice, while Assemblage 4b with only 16 patches covered 4.54 m^2.

In most cases, the mean size of a single patch varied between 0.002 and 1 m^2 for each assemblage across the sides. This must be interpreted with caution, since one big patch can significantly enlarge the mean patch size. The significance of these assumptions was tested with a Friedman's test for all patch sizes across sides and periphery. For Assemblages 1, 2b, 4a and the substrata, there was no significant difference in patch size between the sides ($p>0.05$). Outliers were removed for Assemblages 3 and 4b, after which they did not show a significant difference. Assemblage 2a, however, showed significant differences between the sides ($p<0.001$). This was mainly due to the presence of very large patches on the West side and, to a lesser extent, to those present on the North side of the edifice.

Different correlations were observed between the percentage coverage of the

assemblages. Substratum 1a was negatively correlated with Assemblage 2b (R^2=0.73, p=0.014). Substratum 2 was negatively correlated with Assemblage 2a (R^2=0.67, p=0.023), but positively correlated with Assemblage 3 (R^2=0.73, p=0.014). Assemblage 2a was positively correlated with Assemblage 2b (R^2=0.67, p=0.023) and negatively correlated with Assemblage 3 (R^2=0.73, p=0.014). The other correlations were not significant.

The ordinations (Fig. 4) showed the same trends as observed on the faunal distribution maps. The different sides were plotted based on the relative percentage coverage of the different assemblages and substrata. The constraints added in the canonical analysis were the number of visible active features per square meter. Major trends were maintained in both PCA and RDA analyses (therefore only RDA is shown, Fig. 4a). On the RDA, almost 62% of the variance was explained by the two axes, with axis 1 explaining 51.8% of the variance. The first axis was able to discriminate the more active (East side, southern periphery (S_periph)) from the less active (North side, northern periphery (N_periph) and West side) sides. The main separation in the ordination plot was caused by Assemblages 2a and 2b on the one hand and Assemblage 4a, 4b and Substratum 1a and 2 on the other. The activity features (black smokers, flanges and diffusion zones) also confirmed the separation of the active and less active sides (Fig. 4a). Two sides of the edifice appeared to be in the middle of the ordination plot, namely the South side and the western periphery (W_periph). The cluster analysis, based on Ward's method, clarified this (Fig. 4b), showing that the western periphery is more similar to the North side, the northern periphery and the West side. The South side grouped with the East side and the southern periphery, although the similarity was quite low.

Analysis of video images revealed some preliminary trends regarding which assemblages thrive in or can tolerate warm water flows. Most of these trends were confirmed when the distance from a fluid exit to a patch was measured (Fig. 5). A selection of assemblages were found in close proximity (<1m) to the fluid exits. However, only

Assemblage 3 and Substratum 2 seemed to prevail in the warm water flow. Assemblage 1 was always present in the surroundings of fluid exits, but was rarely seen in the warm water flow itself. The minimum distances of these three assemblages to the closest fluid exit were significantly different from the other assemblages (ANOVA, R^2=0.38, p=0.00). Assemblages with smaller mussels (2a and 2b) were situated further away from the fluid exits. However, for all the sides of the edifice, the assemblage covered with microbial mats (2b) was closer to the fluid exits than the one without (2a). In general, larger patches had a greater probability that their borders are surrounded by different fluid exits.

If a division was made between the different types of fluid exits, black smokers (up to 324°C) and flanges and diffusion zones (<200°C) (Fig. 5 a-b respectively), it was clear that they showed the same trends. Assemblage 3 was found closest to all three types of fluid exits. Assemblage 1 and Substratum 2 showed a similar distribution. The minimum distance of these three assemblages in relation to black smokers was significantly different from that of the other assemblages, while for the flanges and diffusion zones the differences were less obvious. Overall, the minimum distance to flanges and diffuse emissions was half of that to black smokers.

3.5. Neighbouring patterns

Based on video observations, systematic patterns between different neighbouring assemblages appeared to be present. This was confirmed with the analysis of adjacent patches. For the “mussel-based” assemblages, a clear gradient from bare surface with new recruits and scattered mussels (Assemblages 4a and b) to mussel clumps (Assemblages 2a and b) and dense mussel beds (Assemblage 1) was noted. This coincided with an increase in temperature measured in these mussel-based assemblages, respectively ranging from 4.7°C to 12.5°C (Sarrazin et al. in prep).

Each assemblage had at least 2 “preferred” or dominant neighbours, accounting for the occupancy of ca. 50% and more of the adjacent patches (Table 3). The other ca. 50% was divided between the other assemblages and substratum types (n-2=7 with n=9 being the total number of assemblages and substrata). For example, newly formed surface (Substratum 2) was more often bordered by Assemblage 1 and 2a, while Assemblage 3 was more often bordered by Substratum 2 and Assemblage 1. For Assemblages 4a and b, Assemblages 2a and b are the most frequent neighbours.

4. DISCUSSION

In contrast to the diverse assemblages of tubeworms, clams and polychaetes found at hydrothermal vents on the East Pacific Rise (EPR), the shallower vents of the slow-spreading MAR (<2300m depth) are dominated visually, on macrofaunal scales, either by an assemblage of Bathymodiolin mussels (Van Dover, 1995; Turnipseed et al., 2003) or Alvinocaridid shrimps (Desbruyères et al., 2001). Due to the shallower depth of some of these Atlantic vents (e.g. Lucky Strike) and the associated phase separation (i.e. the local pressure-temperature characteristics determine the rate of precipitation of dissolved and particulate metals and sulfide), the hydrothermal fluids lose part of their toxicity, which allows non-vent bathyal fauna to make predatory incursions (Desbruyères et al., 2000). Fishes have been observed to feed on shrimps, crabs and mussels (Saldanha and Biscoito, 1997; Marques and Porteiro, 2000; Desbruyères et al., 2006).

Crucial to our understanding of global macro-ecological patterns are small-scale ecological forcing factors. In particular, the relationships between the substrata, vent activity, fluid flow, temperature and biological tolerances are important. Mid-Atlantic vents differ substantially from those on the EPR in the nature of their abiotic variables. Elucidating the influences of these variables on composition and zonation patterns is one of the main goals of

387 this study. Using a high-resolution video imaging technique, assemblages were identified and
388 mapped on a typical MAR vent edifice, revealing the potential spatial patterns in relation to
389 visible abiotic factors.
390
391 **4.1. Spatial and zonation patterns**
392 When the spatial patterns of the assemblages and substrata were analysed, a systematic
393 lateral zonation between the patches was observed, transforming one assemblage into another
394 over distance. Analyzing the occupancy of neighbouring patches was considered the most
395 appropriate way to quantify the number of transfers. A zonation model, summarising the way
396 that assemblages and substrata change across the edifice, is presented in Fig. 6a. The overall
397 driver of this spatial shift in faunal composition is the decrease in fluid flow, i.e. the presence
398 of high temperature fluid exits and proximity to fluid exits (Fig. 6b). Associated with this
399 decrease in flow is the probable decrease in temperature, sulfide and other associated
400 chemicals. Thermal conditions and associated factors like fluid flow play a role in habitat
401 selection, spatial partitioning and distribution of vent animals (Sarrazin et al., 1999; Bates et
402 al., 2005; Levesque et al., 2006; Mills et al., 2007). An idealized scenario of faunal
403 distribution and zonation at Eiffel Tower is shown in Fig.7.
404 Faunal assemblages can be divided into three groups (Fig. 6). Assemblages 3 and 1 are
405 associated with the harshest environment. Assemblages 2a and 2b, the most abundant on the
406 edifice, are associated with intermediate conditions and are found at moderate distances from
407 fluid-flow exits. Assemblages 4a and 4b can be regarded as the “recolonisation pools” for the
408 rest of the sulfide structure, hosting new recruits and small mytilids. This sequence of
409 assemblages creates a gradient in mussel densities. Among the substrata, Substratum 2 is
410 characterized by the co-occurrence of precipitated anhydrite and shimmering water suggesting
411 the presence of a high permeability. Substratum 1b is colonised by microbial mats and is more

412 abundant at a greater distance from the fluid exits. A spatial segregation between different
413 microbial communities (present in Assemblages 2b, 4b, Substratum 1b and 2) may be a
414 response to a temperature gradient. In addition, the existence of intra-specific (between
415 mussels) and inter-specific (bacteria and mussels, mussels and shrimp) competition for access
416 to resources (e.g. sulfide) could play a role in structuring the spatial distribution of the
417 different communities.

418 The main interacting factors likely to drive the observed assemblage and substratum
419 distribution and zonation are thus twofold, namely abiotic constraints and biotic interactions.
420 Based on experimental manipulations, abiotic gradients and biotic interactions are believed to
421 act jointly to shape benthic vent communities (Micheli et al., 2002, Lenihan et al., 2008).
422 Abiotic constraints include the geomorphology, porosity and composition of the substratum as
423 well as the presence/absence and proximity of fluid exits. Although they were not tested in the
424 present study, biotic interactions must exert an important control on the observed distribution
425 of the fauna (Shank et al. 1998, Sarrazin et al. 2002, Mullineaux et al. 2003). They include the
426 community induced changes in microhabitat, e.g. changes in sulfide concentrations resulting
427 from biological uptake and dilution (Johnson et al., 1994), competition and predator-prey
428 interactions (Micheli et al., 2002). Their exact role and importance, however, is difficult to
429 asses based on imagery.

430 Mussels may out-compete other sessile chemosynthetic macrofauna for access to vent
431 fluid (Lenihan et al., 2008). They have several advantages over other vent animals. For
432 example, dense mussel beds are able to redirect the fluid flow horizontally (Johnson et al.,
433 1994) explaining the existence of vast mussel beds. In addition, their motility enables them to
434 escape from unfavourable environmental conditions or to colonise newly formed habitats.
435 Species of *Bathymodiolus* have been observed moving 0.74cm per hour (Govenar et al., 2004).
436 Temporal evolution studies and manipulative experiments are needed to test these hypotheses

437 and to enhance our knowledge with regard to assemblage dynamics.

438

439 **4.2. Assemblages on the Eiffel Tower edifice**

440 4.2.1. Mussel-based assemblages

441 The dominant megafaunal species, and the main constituent of Assemblages 1, 2a and
442 2b, is *Bathymodiolus azoricus*. *Bathymodiolus* is the most widespread genus in deep-sea
443 chemosynthetic environments, present in both cold seeps and hydrothermal vents (Tyler and
444 Young, 1999). The definition of the assemblages is partially based on a visible difference
445 between big and small mussels that was confirmed by length measurements. In the case of
446 Eiffel Tower, the mussels belonging to a larger size class form dense mussel beds
447 (Assemblage 1) and are relatively more abundant, compared to Assemblages 2a and 2b
448 (mussel clumps), on the more active sides. On all sides of the edifice, a spatial segregation of
449 the assemblages based on their proximity to fluid exits is observed.

450 Larger mussels (Assemblage 1) are found in the close proximity of a fluid exit,
451 suggesting that they may be able to survive a somewhat more hostile environment than the
452 smaller-sized mussels (Desbruyères et al., 2001). The observations presented here support a
453 spatial segregation of mytilid sizes at Eiffel Tower as described previously (Comtet and
454 Desbruyères, 1998; Sarradin et al., 1999; Desbruyères et al., 2001). In contrast to the present
455 observations, the mussels in the Lau Basin (SW Pacific) live further away from the fluid exits.
456 Zonation studies show *Bathymodiolus brevior* to have a low thermal tolerance but a high
457 autotrophic capacity. Like *B. azoricus*, *B. brevior* avoids direct contact with vent fluids,
458 although it can stand high concentrations of sulfide (Henry et al., 2008; Waite et al. 2008).

459 Mytilids use their byssus threads to attach to the substratum, which allows them to
460 grow almost everywhere on the edifice and to connect to other individuals, resulting in
461 'stacking' several layers deep (Johnson et al., 1994). In this regard, the permeability of the

462 substratum and the thermal tolerance of the animals appear to play a significant role in the
463 faunal distribution observed. Shrimps (Assemblage 3) can get closest to the fluid exits. They
464 are very mobile, are not attached to the substratum and have a temperature resistance up to
465 36°C (Shillito et al., 2006). Therefore they can survive on the highly permeable substrata
466 close to the fluid exits (e.g. Substratum 2). This is supported by the positive correlation
467 between Substratum 2 and Assemblage 3. Mussels, on the other hand, are not observed on
468 newly formed surfaces, either because they have more difficulties attaching to this substratum
469 or they are less tolerant of warm fluid flows.

470 The dependence of the mussel community on the lateral dispersion of vent fluids by
471 the physical structure of the community makes individuals at the boundaries vulnerable to a
472 disruption in reduced chemical supply. A limit to autotrophy would constrain the growth rates
473 within the vent environment, enhancing the spatial segregation between large and small sizes
474 and their proximity to fluid exits. We speculate that individuals living closer to fluid exits
475 could have a faster growth rate, or are able to attain larger sizes because there is no limit to
476 sulfide and methane (see Bergquist et al., 2004 on *Bathymodiolus childressi* at cold seeps).

477 In the Pacific hydrothermal vents *Bathymodiolus* species are regarded as the final
478 survivors in waning vent fields. When the activity decreases they tend to out-compete the
479 siboglinid tubeworms (Hessler at al., 1985). Mussel beds offer a complex secondary surface
480 and interstitial microhabitats for associated species (Van Dover and Trask, 2000). The
481 provision of complex physical structures by foundation species plays a role in the
482 composition and diversity of vent communities. It contributes to altering the physico-chemical
483 environment, and thus influences the physiology of the organisms (Bergquist et al., 2004;
484 Govenar and Fisher, 2007). Although naturally high densities of mussels can directly or
485 indirectly inhibit recruitment of invertebrates at deep-sea hydrothermal vents (Lenihan et al.,
486 2008), gastropod grazers are found on the mussel shells, possibly feeding on the microbial

cover. In addition, some gastropod species at other vent sites have been observed to (re)position themselves along thermal gradients, looking for the ideal temperature regime (Bates et al., 2005; Mills et al., 2007).

New mytilid recruits occur on the mussel shells in the other assemblages and in larger numbers on bare substratum in Assemblage 4, which is present on all sides, tower and periphery, of the edifice, mostly at the base. Assemblage 4 can be either closer to lower temperature exits (e.g. flanges, diffuse flow) or further away from high temperature black smokers. Often dead mussel shells can be encountered in the immediate vicinity. A change in the porosity of the substratum or local (de)activation might explain this observation.

Decapod predators and scavengers (*Segonzacia mesatlantica, Mirocaris fortunata, Chorocaris chacei* and *Alvinocaris markensis*) are all very mobile and can occur anywhere on the edifice, but they are most abundant in the more hydrothermally-active zones. *Segonzacia mesatlantica* appears to require rougher vertical substrata onto which they can grip, or horizontal platforms from which they cannot slip off, or mussel beds that provide ample support.

4.2.2. Shrimp assemblage

The occurrence of shrimp (Assemblage 3) is an indication for the proximity of vent fluid exits since they are usually present in the warm water flow. The higher abundance of Alvinocarididae on the more active East and South sides and the peripheral zones can be explained by the higher hydrothermal activity observed there. At Eiffel Tower, the shrimps may be predators and/or scavengers, consuming free-living bacteria present in the hydrothermal solution flows or ingesting other small invertebrates (Gebruk et al., 2000; Colaço et al., 2002). Shrimps also exhibit a more opportunistic behaviour as they can be observed feeding on broken mussel shells. *Segonzacia mesatlantica* consumes shrimps and

512 other small invertebrates (Voight, 2000; Colaço et al., 2002) and were also abundantly present
513 at broken mussel shell sites. *Mirocaris fortunata* is present in almost all samples taken at
514 Eiffel Tower (Sarrazin et al., in prep.) suggesting that they live in the interstitial spaces
515 between the mytilids or hidden in the cracks and crevices from which fluids enriched in
516 micro-organisms can be emanating.
517

518 **4.3. Comparison between the edifice sides**

519 The hydrothermally most active sides of Eiffel Tower show a lower degree of
520 colonisation and share a similar composition. Analogously the less active sides display a high
521 degree of colonisation with a comparable composition. However, if there is no hydrothermal
522 activity there is no visible vent-associated fauna. While carrying out video-transects, the
523 temperature sensor on the ROV Victor registered up-welling clouds of hot fluids present at
524 East and South sides and the highest temperature was reached at the top of the edifice. Similar
525 patterns were observed for the North and West sides but the temperature differences were
526 considerably smaller than on the more active sides (ca. 1.2°C for the North and West sides
527 compared to 4°C for the East and South sides). The sides that were considered the most active
528 showed the highest temperatures, linking temperature with flow vigour as already suggested by
529 Sarrazin et al. (1997) for the Pacific.

530 The highest percentage of colonisation can be found on the West side of the edifice.
531 The mussel shells are mostly of a smaller size range than on the other sides (dominance of
532 Assemblages 2a and 2b; Fig. 3h). Many mussels on the West side were observed with their
533 siphons opening upwards. This might be explained by the fact that *Bathymodiolus azoricus* is
534 capable of filter feeding, in addition to supporting a nutritional relationship with the bacterial
535 symbionts in its gill tissue (Tunnicliffe, 1991; Colaço et al., 2002). The limited supply of
536 hydrothermal fluids and reduced chemicals on the West side might constrain their growth,

explaining the high abundance of smaller sized individuals on this side. According to a carbon-flux model developed by Martins et al. (2008), small mussels depend more on filter feeding than big mussels, which rely mostly on chemosynthesis.

The western periphery is fairly active compared to the tower. We suggest that the West side tower is less permeable since there are almost no fluid exits. Fluids may have been redirected towards the periphery because the main tower was partially clogged. The south peripheral zone is very active and shows a low degree of colonisation. The percentage of colonisation is equally divided between the different faunal assemblages (1, 2a, 2b and 3 – Fig. 3(h)). Individuals of *B. azoricus* living in this zone are quite large (≥4cm). Most likely these adults originate from the main tower 1 or 2m away.

4.4. Habitat and substrata

Hydrothermal vent fields and sites are very changeable environments. Unlike the high frequency of eruptive events on fast-spreading ridges, drastic changes in the Atlantic Ocean are rather rare (Van Dover, 1995), but a certain degree of (sulfide) accretion is responsible for some structural changes (Haymon et al., 1983), providing additional substrata for fauna to occupy (Copley et al., 1997; Sarrazin et al., 1997; Butler et al., 1998). Some of these rapid accretions are responsible for certain over-night changes in the appearance of the Eiffel Tower edifice.

The presence of shimmering water and even black smokers at the base and the peripheral zones could be explained by the redirection of the fluids. During the life span of a hydrothermal vent, the edifice can become clogged by mineral precipitation. Sulfide deposition causes loss of pore connectivity in the sediment, thus drastically reducing the substratum permeability and fluid flow rate (Zhu et al., 2007). The fluids may be redirected towards the periphery, as observed on Juan de Fuca Ridge (Sarrazin et al., 1997).

562 The colour of the substratum can depend on the nature of the minerals precipitating
563 from the vent fluids. Substratum 1a has no visible mineral precipitation and is unable to
564 support vent-endemic fauna, probably because it is not permeable, i.e. no hot fluids can seep
565 through. It can be present as small patches between the faunal assemblages or as larger
566 patches further away from the fluid exits and nearly always at the base of the structure. In
567 contrast, Substratum 2, which is characterised by obvious anhydrite precipitation, appears to
568 be permeable, letting warm fluids flow through. It often seems to act as a buffer zone between
569 the fluid exits and the faunal patches. Substratum 1b can be covered by thick microbial mats
570 that can serve as a feeding ground for grazing organisms further away from the fluid exits.
571 The nature of the substratum (porosity, composition and instability) may play an important
572 role in structuring vent assemblages and its importance should not be underestimated
573 (Tunnicliffe, 1991; Grehan and Juniper, 1996; Copley et al., 1997; Shank et al., 1998;
574 Sarrazin et al., 2002; Tsurumi and Tunnicliffe, 2003; Zhu et al., 2007).
575

576 ## 5. CONCLUSION

577 Our study has revealed a patchy zonation of biological assemblages around fluid exits
578 on the Eiffel Tower hydrothermal construct (Fig. 7). A fluid exit is always bordered by
579 Substratum 2 that can be colonised by shrimps (transforming into Assemblage 3) followed by
580 larger-sized mussels (Assemblage 1). Beyond this point, a decrease in mussel densities and
581 sizes occurs with increasing distance from the fluid exits (Assemblages 2 to Assemblages 4)
582 as well as an increase in the area of bare surface between the mussel clumps. A gradient is
583 thus created by the presence or absence of fluid exits and the fluid flow dynamics. This
584 implies a spatial segregation of assemblages based on proximity to fluid exits and correlated
585 environmental factors. As a result, there is a greater similarity in the percentage coverage of
586 faunal assemblages and substrata between the highly active sides of the hydrothermal edifice.

The same relationship applies to the less active sides. The influence of factors such as geomorphology and porosity of the substrata on assemblage distribution should not be underestimated. These can constrain the ability of fauna to colonise certain regions. Biological interactions are another likely factor influencing faunal distributions, although their importance is difficult to verify based on imagery.

Acknowledgments

We would like to thank Captain P. Guillemet of the R/V Pourquoi pas? and his crew for their collaboration indispensable to the success of the MoMARETO cruise. We also acknowledge the Victor 6000 ROV pilots for their patience and constant support. Part of MoMARETO was funded by the EXOCET/D European project, contract # GOCE-CT-2003-505342. We are grateful to P-M Sarradin, second chief scientist on the MoMARETO cruise for his help and ideas, H. Ondréas for the kind assistance with the creation of the maps of the MAR and Eiffel Tower. The PhD project has been carried out in the framework of the MarBEF Network of Excellence 'Marine Biodiversity and Ecosystem Functioning' which is funded by the Sustainable Development, Global Change and Ecosystems Programme of the European Community's Sixth Framework Programme (contract no. GOCE-CT-2003-505446). This publication is contribution number MPS-09020 of MarBEF. Thanks to ANR “DeepOases” for extra financial support. IMARDOP/UAz is Research and Development Unit #531 and ISR-Associated Laboratory #9 funded by the Portuguese Foundation for Science and Technology (FCT) through pluri-annual and programmatic funding schemes (FEDER, POCI2001, FSE) and by the Azores Directorate for Science and Technology (DRCT). This manuscript also benefited from the constructive comments of three anonymous reviewers and associate editor Andy Gooday.

References

Bates, A.E., Tunnicliffe, V., Lee, R.W., 2005. Role of thermal conditions in habitat selection by hydrothermal vent gastropods. Mar. Ecol. Prog. Ser. 305, 1-15

Bergquist, D.C., Fleckenstein, C., Szalai, E.B., Knisel, J., Fisher, C.R., 2004. Environment drives physiological variability in the cold seep mussel *Bathymodiolus childressi*. Limnol. Oceanogr. 49, 706-715

Butler, I.B., Fallick, A.E., Nesbitt, R.W., 1998. Mineralogy, sulphur isotope geochemistry and the development of sulfide structures at the Broken Spur hydrothermal vent site, 29°10' N, Mid-Atlantic Ridge. J. Geol. Soc. 155, 773-785

Charlou, J.L., Dental, J.P., Douville, E., Jean-Baptiste, P., Radford-Knoery, J., Fouquet, Y., Dapoigny, A., Stievenard, M., 2000. Compared geochemical signatures and the evolution of Menez Gwen (37° 50' N) and Lucky Strike (37°17' N) hydrothermal fluids, South of the Azores Triple Junction on the Mid-Atlantic Ridge. Chem. Geol. 171, 49-75

Chevaldonne, P., Jollivet, D., 1993. Videoscopic study of deep-sea hydrothermal vent alvinellid polychaete populations - biomass estimation and behavior. Mar. Ecol. Prog. Ser. 95, 251-262

Colaco, A., Desbruyeres, D., Comtet, T., Alayse, A.M., 1998. Ecology of the Menez Gwen hydrothermal vent field (Mid-Atlantic Ridge Azores Triple Junction). Cah. Biol. Mar. 39, 237-240

Colaco, A., Dehairs, F., Desbruyeres, D., 2002. Nutritional relations of deep-sea hydrothermal fields at the Mid-Atlantic Ridge: a stable isotope approach. Deep-Sea Res. I 49, 395-412

Comtet, T., Desbruyeres, D., 1998. Population structure and recruitment in mytilid bivalves from the Lucky Strike and Menez Gwen hydrothermal vent fields (37° 17' N and 37° 50' N on the Mid-Atlantic Ridge). Mar. Ecol. Prog. Ser. 163, 165-177

Copley, J.T.P., Tyler, P.A., Murton, B.J., Van Dover, C.L., 1997. Spatial and interannual variation in the faunal distribution at Broken Spur vent field (29° N, Mid-Atlantic Ridge). Mar. Biol. 129, 723-733

Copley, J.T.P., Jorgensen, P.B.K., Sohn, R.A., 2007. Assessment of decadal-scale ecological change at a deep Mid-Atlantic hydrothermal vent and reproductive time-series in the shrimp Rimicaris exoculata. J. Mar. Biol. Assoc. UK 84, 859-867

Desbruyeres, D., Almeida, A., Biscoito, M., Comtet, T., Khripounoff, A., Le Bris, N., Sarradin, P.M., Segonzac, M., 2000. A review of the distribution of hydrothermal vent communities Along the northern Mid-Atlantic Ridge: dispersal vs. environmental controls. Hydrobiologia 440, 201-216

Desbruyeres, D., Biscoito, M., Caprais, J.C., Colaco, A., Comtet, T., Crassous, P., Fouquet, Y., Khripounoff, A., Le Bris, N., Olu, K., Riso, R., Sarradin, P.M., Segonzac, M., Vangriesheim, A., 2001. Variations in deep-sea hydrothermal vent communities on the Mid-Atlantic Ridge near the Azores plateau. Deep-Sea Res. I 48, 1325-1346

650 Desbruyeres, D., Segonzac, M., Bright, M., (eds) 2006. Handbook of deep-sea hydrothermal
651 vent fauna. Second completely revised edition. Denisia, 18. Biologiezentrum der
652 Oberösterreichischen Landesmuseen. Linz, Austria
653 Fabri, M.C., Galéron, J., Larour, M., Maudire, G., 2006. Combining the Biocean database for
654 deep-sea benthic data with the online Ocean Biogeographic Information System. Mar.
655 Ecol. Prog. Ser. 316, 215–224
656 Fouquet, Y., Eissen, J.P., Ondreas, H., Barriga, F., Batiza, R., Danyushevsky, L., 1998.
657 Extensive volcaniclastic deposits at the Mid-Atlantic Ridge axis: results of deep-water
658 basaltic explosive volcanic activity? Terra Nova 10, 280-286
659 Fustec, A., Desbruyères, D., Juniper, K.S., 1987. Deep-sea hydrothermal vent communities at
660 13°N on the East Pacific Rise: Microdistribution and temporal variations. Biol. Oceanogr.
661 4(2), 121-164
662 Gebruk, A.V., Southward, E.C., Kennedy, H., Southward, A.J., 2000. Food Sources,
663 behaviour, and distribution of hydrothermal vent shrimps at the Mid-Atlantic Ridge. J.
664 Mar. Biol. Assoc. UK 80, 485-499
665 Govenar, B., Freeman, M., Bergquist, D.C., Johnson, G.A., Fisher, C.R., 2004. Composition
666 of a one-year-old *Riftia pachyptila* community following a clearance experiment: insight
667 to succession patterns at deep-sea hydrothermal vents. Biol. Bull. 207, 177–182.
668 Govenar, B., Le Bris, N., Gollner, S., Glanville, J., Aperghis, A.B., Hourdez, S., Fisher, C.R.,
669 2005. Epifaunal community structure associated with *Riftia pachyptila* aggregations in
670 chemically different hydrothermal vent habitats. Mar. Ecol. Prog. Ser. 305, 67-77
671 Govenar, B., Fisher, C.R., 2007. Experimental evidence of habitat provision by aggregations
672 of *Riftia pachyptila* at hydrothermal vents on the East Pacific Rise. Mar. Ecol. Evol.
673 Persp. 28, 3-14
674 Grehan, A.J., Juniper, S.K., 1996. Clam distribution and subsurface hydrothermal processes at
675 Chowder Hill (Middle Valley), Juan De Fuca Ridge. Mar. Ecol. Prog. Ser. 130, 105-115
676 Haymon, R.M., 1983. Growth history of hydrothermal black smoker chimneys. Nature 301,
677 695-698
678 Henry, M.S., Childress, J.J., Figueroa, D., 2008. Metabolic rates and thermal tolerances of
679 chemoautotrophic symbioses from Lau Basin hydrothermal vents and their implications
680 for species distributions. Deep-Sea Res. I 55, 679–695
681 Hessler, R.R., Smithey, W.M., Keller, C.H., 1985. Spatial and temporal variation of giant
682 clams, tube worms and mussels at deep-sea hydrothermal vents. Biol. SOC. Wash. Bull. 6,
683 411-428.
684 Hessler, R.R., Smithey, W.M., Boudrias, M.A., Keller, C.H., Lutz, R.A., Childress, J.J., 1988.
685 Temporal change in megafauna at the Rose Garden hydrothermal vent (Galapagos Rift -
686 Eastern Tropical Pacific). Deep-Sea Res. A 35, 1681- 1710
687 Humphris, S.E., Fornari, D.J., Scheirer, D.S., German, C.R., Parson, L.M., 2002. Geotectonic

688 setting of hydrothermal activity on the summit of Lucky Strike seamount (37°17' N, Mid-
689 Atlantic Ridge). Geochem. Geophys. Geosyst. 3(8)
690 Johnson, K.S., Childress, J.J., Beehler, C.L., Sakamoto, C.M., 1994. Biogeochemistry of
691 hydrothermal vent mussel communities - the deep-sea analog to the intertidal zone. Deep-
692 Sea Res. I 41, 993-1011
693 Jollivet, D., 1993. Distribution et evolution de la faune associee aux sources hydrothermales
694 profondes a 13”N sur la dorsale du Pacifique oriental: le cas particulier des polychetes
695 Alvinellidae. PhD thesis, Université Bretagne Occidentale, Brest, France
696 Langmuir, C., Humphris, S., Fornari, D., Van Dover, C., Von Damm, K., Tivey, M.K.,
697 Colodner, D., Charlou, J.L., Desonie, D., Wilson, C., Fouquet, Y., Klinkhammer, G.,
698 Bougault, H., 1997. Hydrothermal vents near a mantle hot spot: the Lucky Strike vent
699 field at 37° N on the Mid-Atlantic Ridge. Earth Planet Sci. Lett. 148, 69-91
700 Lenihan, H.S., Mills, S.W., Mullineaux, L.S., Peterson, S.H., Fisher, C.R., Micheli, F., 2008.
701 Biotic interactions at hydrothermal vents: Recruitment inhibition by the mussel
702 Bathymodiolus thermophilus. Deep-Sea Res. I 55, 1707–1717
703 Levesque, C., Juniper, S.K., Limen, H., 2006. Spatial organization of food webs along habitat
704 gradients at deep-sea hydrothermal vents on Axial Volcano, Northeast Pacific. Deep-Sea
705 Res. I 53, 726-739
706 Limen, H., Juniper, S.K., 2006. Habitat controls on vent food webs at Eifuku Volcano,
707 Mariana Arc. Cah. Biol. Mar. 47, 449-455
708 Luther, G.W., Rozan, T.F., Taillefert, M., Nuzzio, D.B., Di Meo, C., Shank, T.M., Lutz, R.A.,
709 Cary, S.C., 2001. Chemical speciation drives hydrothermal vent ecology. Nature 410,
710 813-816
711 Martins, I., Colaço, A., Dando, P.R., Martins, I., Desbruyères, D., Sarradin, P.M., Marques,
712 J.C., Serrão-Santos, R., 2008. Size-dependent variations on the nutritional pathway of
713 *Bathymodiolus azoricus* demonstrated by a C-flux model. Ecol. Model. 217, 59-71
714 Marques, A., Porteiro, F., 2000. Hydrothermal vent mussel *Bathymodiolus* sp (Mollusca:
715 Mytilidae): diet item of *Hydrolagus affinis* (Pisces: Chimaeridae). Copeia 3, 806-807
716 Micheli, F., Peterson, C.H., Mullineaux, L.S., Fisher, C.R., Mills, S.W., Sancho, G., Johnson,
717 G.A., Lenihan, H.S., 2002. Predation structures communities at deep-sea hydrothermal
718 vents. Ecol. Monogr. 72:365-382
719 Mills, S.W., Mullineaux, L.S., Tyler, P.A., 2007. Habitat associations in gastropod species at
720 East Pacific Rise hydrothermal vents (9° 50' N). Biol. Bull. 212, 185-194
721 Mullineaux, L.S., Peterson, C.H., Micheli, F., Mills, S.W., 2003. Successional mechanism
722 varies along a gradient in hydrothermal fluid flux at deep-sea vents. Ecol. Monogr. 73,
723 523-542
724 Oksanen, J., Kindt, R., Legendre, P., O'Hara, B., Simpson, G.L., Solymos, P., Stevens,
725 M.H.M., Wagner, H., (2008). vegan: Community Ecology Package. R package version

726 1.15-0. http://cran.r-project.org/, http://vegan.r-forge.r-project.org/
727 Ondreas, H., Fouquet, Y., Voisset, M., Radford-Knoery, J., 1997. Detailed study of three
728 contiguous segments of the Mid-Atlantic Ridge, South of the Azores (37° N to 38° 30' N),
729 using acoustic imaging coupled with submersible observations. Mar. Geophys. Res. 19,
730 231-255
731 Ondréas, H., M. Cannat, Y. Fouquet, A. Normand, P. M. Sarradin, and J. Sarrazin (2009),
732 Recent volcanic events and the distribution of hydrothermal venting at the Lucky Strike
733 hydrothermal field, Mid-Atlantic Ridge, Geochem. Geophys. Geosyst., 10 (2)
734 Saldanha, L., Biscoito, M., 1997. Fishes from the Lucky Strike and Menez Gwen
735 hydrothermal vent sites (Mid-Atlantic Ridge). Bol. Mus. Mun. Funchal 49(283), 189-206.
736 Sarradin, P.M., Caprais, J.C., Riso, R., Kerouel, R., Aminot, A., 1999. Chemical environment
737 of the hydrothermal mussel communities in the Lucky Strike and Menez Gwen vent
738 fields, Mid Atlantic Ridge. Cah. Biol. Mar. 40, 93-104
739 Sarrazin, J., Robigou, V., Juniper, S.K., Delaney, J.R., 1997. Biological and geological
740 dynamics over four years on a high-temperature sulfide structure at the Juan De Fuca
741 Ridge hydrothermal observatory. Mar. Ecol. Prog. Ser. 153, 5-24
742 Sarrazin, J., Juniper, S.K., Massoth, G., Legendre, P., 1999. Physical and chemical factors
743 influencing species distributions on hydrothermal sulfide edifices of the Juan De Fuca
744 Ridge, Northeast Pacific. Mar. Ecol. Prog. Ser. 190, 89-112
745 Sarrazin, J., Levesque, C., Juniper, S.K., Tivey, M.K., 2002. Mosaic community dynamics on
746 Juan De Fuca Ridge sulfide edifices: substratum, temperature and implications for trophic
747 structure. Cah. Biol. Mar. 43, 275-279
748 Shank, T.M., Fornari, D.J., Von Damm, K.L., Lilley, M.D., Haymon, R.M., Lutz, R.A., 1998.
749 Temporal and spatial patterns of biological community development at nascent deep-sea
750 hydrothermal vents (9° 50' N, East Pacific Rise). Deep-Sea Res. II 45:465-515
751 Shillito, B., Le Bris, N., Hourdez, S., Ravauxl, J., Cottin, D., Caprais, J.C., Jollivet, D., Gaill,
752 F., 2006. Temperature resistance studies on the deep-sea vent shrimp Mirocaris fortunata.
753 J. Exp. Biol. 209:945-955
754 Tsurumi, M., Tunnicliffe, V., 2001. Characteristics of a hydrothermal vent assemblage on a
755 volcanically active segment of Juan De Fuca Ridge, Northeast Pacific. Can. J. Fisheries
756 Aquat. Sci. 58, 530-542
757 Tsurumi, M., Tunnicliffe, V., 2003. Tubeworm associated communities at hydrothermal vents
758 on the Juan De Fuca Ridge, Northeast Pacific. Deep-Sea Res. I 50, 611-629
759 Tunnicliffe, V., 1991. The biology of hydrothermal vents - ecology and evolution. Oceanogr.
760 Mar. Biol. 29, 319-407
761 Turnipseed, M., Knick, K.E., Lipcius, R.N., Dreyer, J., Van Dover, C.L., 2003. Diversity in
762 mussel beds at deep-sea hydrothermal vents and cold seeps. Ecol. Lett. 6, 518-523
763 Tyler, P.A., Young, C.M., 1999. Reproduction and dispersal at vents and cold seeps. J. Mar.

764 Biol. Assoc. UK 79, 193-208
765 Van Dover, C.L., 1995. Ecology of Mid-Atlantic Ridge hydrothermal vents. In: Parson, L.M.,
766 Walker, C.L., Dixon, D.R. (Eds.), Hydrothermal vents and processes, Spec Publ 87.
767 Geological Society, London, pp. 257–294
768 Van Dover, C.L., Trask, J.L., 2000. Diversity at deep-sea hydrothermal vent and intertidal
769 mussel beds. Mar. Ecol. Prog. Ser. 195, 169-178
770 Voight, J.R., 2000. A review of predators and predation at deep-sea hydrothermal vents. Cah.
771 Biol. Mar. 41, 155-166
772 Waite, T.J., Moore, T.S., Childress, J.J., Hsu-Kim, H., Mullaugh, K.M., Nuzzio, D.B.,
773 Paschal, A.N., Tsang, J., Fishers, C.R., Luther, G.W., 2008. Variation in sulfur speciation
774 with shellfish presence at a Lau Basin diffuse flow vent site. J. Shellfish Res., 27, 163-168
775 Zhu, W.L., Tivey, M.K., Gittings, H., Craddock, P.R., 2007. Permeability-porosity
776 relationships in seafloor vent deposits: dependence on pore evolution processes. J.
777 Geophys. Res. Solid Earth 112 (B5)
778
779
780 **Figures**
781
782 Fig. 1. (a) Hydrothermal vent fields of the northern Mid-Atlantic Ridge. The major transform
783 faults are shown as well. Image modified from Desbruyères et al. (2001). (b) Bathymetric
784 map of the Lucky Strike vent field area at a mean depth of 1700m (Flores 1998©Ifremer,
785 resolution: 20m). The Lucky Strike vent field consists of 3 seamounts surrounding a lava lake.
786 (c) Microbathymetric map of Eiffel Tower (MoMARETO 2006©Ifremer, resolution=20cm),
787 which is situated in the south-eastern region, on the saddle between two seamounts. (d)
788 Terminology of the different sides used in this study.
789
790 Fig. 2. Faunal assemblages identified at Eiffel Tower hydrothermal edifice. (a) Assemblage 1:
791 Dense *Bathymodiolus azoricus* beds (the mussels are of the larger size class, in general > 4cm),
792 occasionally patchy microbial mats can be present. (b) Assemblage 2a: *Bathymodiolus*
793 *azoricus* clumps (in this case the mussels are almost always less than 4cm in length) separated
794 by bare surface without visible microbial mats or (c) Assemblage 2b: with visible microbial
795 mats. (d) Assemblage 3: Bare surface ‘colonised’ by Alvinocarididae (*Mirocaris fortunata*
796 and/or *Chorocaris chacei*). (e) Bare surface with mussel “veins” and very small mussels
797 (possibly new recruits) without visible microbial mats (Assemblage 4a) and with visible
798 microbial mats (Assemblage 4b). (f) Substratum 1a represents bare dark brownish, sometimes
799 slightly reddish surfaces (with on the image the fish *Gaidropsarus* sp. hiding in a crevice). (g)
800 Substratum 1b represents bare surfaces with visible microbial mats. (h) Substratum 2
801 represents bare surfaces with clear mineral precipitation (whitish, greyish) and with possible

802 microbial presence as well (cf. Table 1). Predators and scavengers (*Segonzacia mesatlantica*
803 (Bythograeidae), *Mirocaris fortunata, Chorocaris chacei* and *Alvinocaris markensis* and some
804 fishes) can be present on top of these assemblages. Scales were not put on the individual
805 pictures due to malfunctioning of the laser pointers during the 2006 cruise. The surface covered
806 by each image depends on the zoom-level, proximity to the edifice and irregularity of the
807 edifice.
808
809 Fig. 3. Spatial distribution of faunal assemblages and substrata on each side of the Eiffel
810 Tower hydrothermal edifice (Lucky Strike vent field, MAR). (a) North side, (b) Northern
811 periphery, (c) Western periphery, (d) West side, (e) South side, (f) Southern periphery, (g)
812 East side and (h) stacked histogram representing the % of coverage per assemblage.
813
814 Fig. 4. Ordinations (canonical analyses) based on the relative percentage coverage of each
815 assemblage and substratum on each side of the Eiffel Tower structure. PCA showed exactly
816 the same tendencies as the RDA and is therefore not shown. (a) Redundancy Analysis (RDA),
817 where the number of visible active features ($n.m^{-2}$) acted as constraints. The horizontal and
818 vertical axes together take into account 61.9% of the variation between the sides, although the
819 horizontal axis is clearly more important. (b) Ward's cluster analysis. Clustering of the
820 different sides of Eiffel Tower based on assemblage coverage. The agglomeration method
821 used was Ward's method which minimizes the Sum of Squares between two formed clusters
822 (the most similar sides cluster together first). The patterns are similar to those revealed by the
823 canonical analysis. The positioning of the South side and the western periphery, which were
824 difficult to interpret in the RDA, are clarified in the cluster analysis (S_periph=southern
825 periphery, N_periph=northern periphery, W_periph=western periphery).
826
827 Fig. 5. Minimum and maximum distances of the assemblages (n=6) and substrata (n=3) were
828 measured to the different activity features and their associated temperature regimes; (a). black
829 smokers (324°C) and (b). flanges and diffusion zones (<200°C).
830
831 Fig. 6. The neighbour transfer patterns between assemblages and substrata are presented in a
832 zonation model (a). For each assemblage the adjacent patches were analysed. This resulted in
833 2 'favourite' neighbours (2 arrows) accounting for more than 50% occupancy of the adjacent
834 patches (cf. Table 3). The primary driving force (b) that coincides with this zonation pattern is
835 shown as well.
836
837 Fig. 7. A conceptual model representing an idealized biological zonation of assemblages and
838 substratum distribution at Eiffel Tower, taking into account all results presented this study.
839 Patches occupied by assemblages and substrata are positioned on the structure in a way that

represents their relative size and positions relative to other assemblages and to the fluid exit. Mean patch sizes are in proportion as well as the relative distance to the fluid exit. Faunal assemblages (1, 2a, 2b, 3, 4a, 4b) are represented by a sketch, substrata are named on the patch itself (Sub 1a, Sub 1b, Sub 2). Some predators are represented as well; *Cataetyx laticeps* (Pisces) is lying at the bottom of the structure, and *Hydrolagus pallidus* (Pisces) is passing by left of the sulfide structure. The presence of the crab, *Segonzacia mesatlantica*, is mostly driven by the presence of a food source.

Tables

Table 1. Composition of the faunal assemblages and substrata as well as several physico-chemical and topographic characteristics, all based on visual observations. Since the identification of the assemblages was based on video imagery, only mega- and macro-faunal species are represented here. Ophiuroids and fish were not included because there was no discernable pattern to their occurrence ++ Abundant, + present, () occasional, - absent. (Ass = Assemblage, Sub = Substratum)

			Ass 1	Ass 2a	Ass 2b	Ass 3	Ass 4a	Ass 4b	Sub 1a	Sub 1b	Sub2
Fauna											
Bivalvia	Mytilidae	*Bathymodiolus azoricus* (Larger sized)	++	(+)	(+)	-	-	-	-	-	-
		Bathymodiolus azoricus (Smaller sized)	(+)	++	++	-	+	+	-	-	-
		Bathymodiolus azoricus (New recruits)	+	+	+	-	+	+	-	-	-
Decapoda	Alvinocarididae	*Mirocaris fortunata*	+	(+)	(+)	++	(+)	(+)	-	(+)	(+)
		Chorocaris chacei	+	(+)	(+)	++	(+)	(+)	-	(+)	(+)
		Alvinocaris markensis	(+)	(+)	(+)	(+)	-	-	-	-	(+)
	Bythograeidae	*Segonzacia mesatlantica*	(+)	(+)	(+)	(+)	(+)	(+)	(+)	(+)	(+)
Gastropoda		Limpets (*Lepetodrilus atlanticus*,P*seudorimula midatlantica, Protolira valvatoides,* etc)	+	+	+	-	++	++	-	-	-
Cnidaria		Hydroids	-	-	-	-	++	-	(+)	-	-
Micro-organisms		Visible microbial mats	(+)	-	++	(+)	-	++	-	++	+
Flow features											
proximity of black smoker			++	+	+	++	-	-	-	-	++
proximity of flange/diffusion zones			++	+	+	++	++	++	-	+	++
in flow			No	No	No	Yes	No	No	No	No	Yes
Habitat charachteristics			possibly everywhere	possibly everywhere	possibly everywhere	possibly everywhere, rougher substrata	Mainly edifice base and periphery	Mainly edifice base and periphery	Mainly edifice base and periphery	possibly everywhere	possibly everywhere

Table 2. Percentage of the edifice that is colonised by fauna and the number of active features (n=black smokers, flanges and diffusion zones) per m² for each side. The least colonised side of the tower (upper 8m) is the most active one and vice versa. The peripheral zones (lower 3m until sea bottom is reached) show similar trends. Highest activity and degree of colonisation values are marked in bold.

Tower	% coverage/colonisation	# active features (n/m²)
East	28.11	**0.84**
South	49.17	**0.60**
West	**82.82**	0.19
North	**58.85**	0.36
Periphery	% coverage/colonisation	# active features (n/m²)
East periphery	0	0
South periphery	12.75	**0.53**
West periphery	**54.10**	**1.16**
North periphery	**64.54**	0.39

Table 3. Representation of the dominant neighbouring patches (2 for each assemblage), responsible for an occupancy of ca. 50% of the adjacent patches.

	Dominant neighbours	***%***	∑
Assemblage 1	Substratum 2	30.8	61.9
	Assemblage 2a	31.1	
Assemblage 2a	Assemblage 2b	20.9	48.8
	Substratum 2	27.9	
Assemblage 2b	Assemblage 2a	40.5	55
	Assemblage 1	14.5	
Assemblage 3	Substratum 2	34.5	64.1
	Assemblage 1	29.6	
Assemblage 4a	Assemblage 2a	32.9	55.9
	Assemblage 2b	23.0	
Assemblage 4b	Assemblage 2a	34	60.4
	Assemblage 2b	26.4	
Substratum 1a	Assemblage 2a	25.7	45.1
	Assemblage 4a	19.4	
Substratum 1b	Assemblage 2a	29.3	55.8
	Assemblage 2b	26.5	
Substratum 2	Assemblage 2a	29.2	56.5
	Assemblage 1	27.3	

Figures

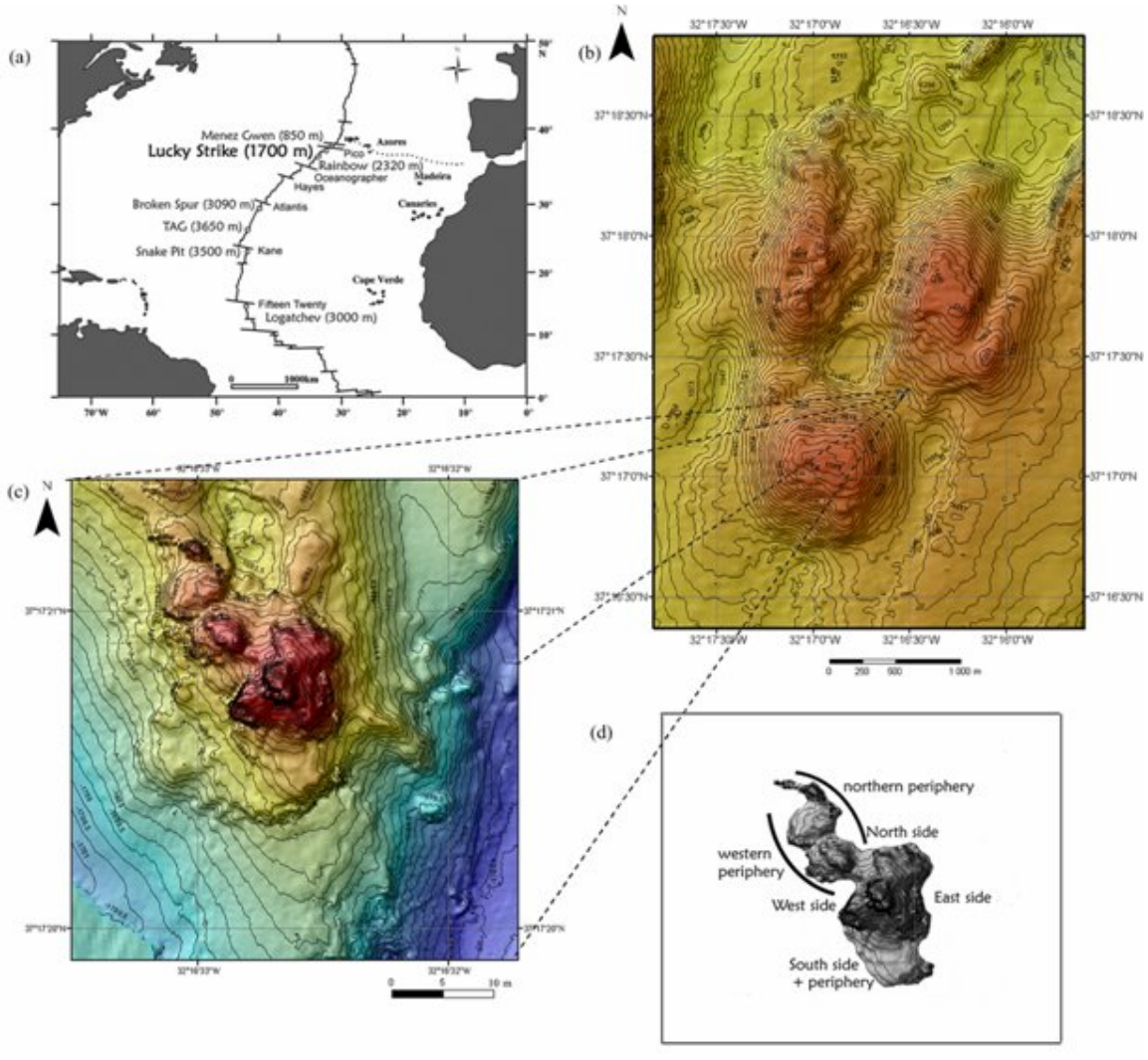

Fig. 1.

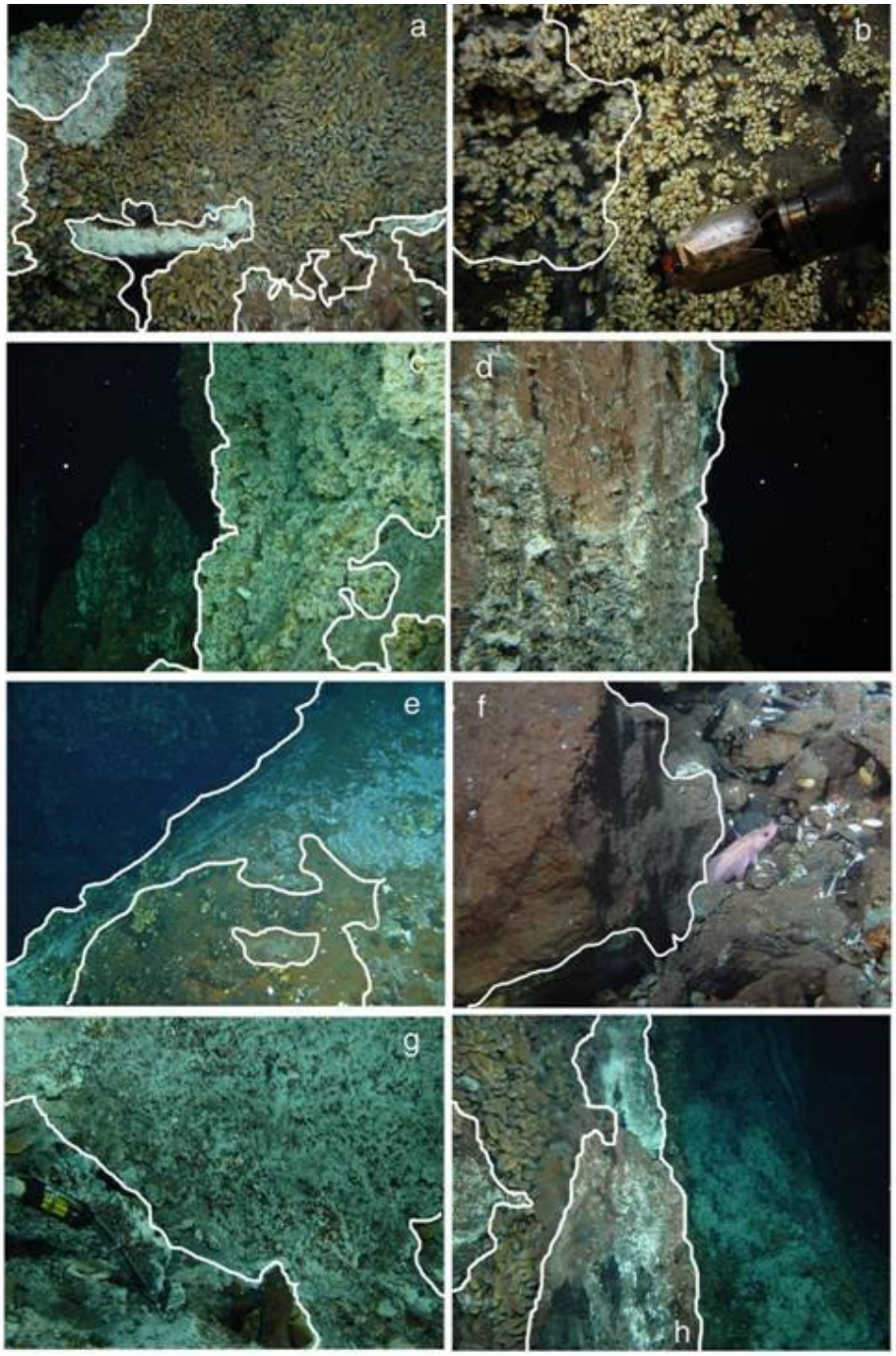

Fig. 2.

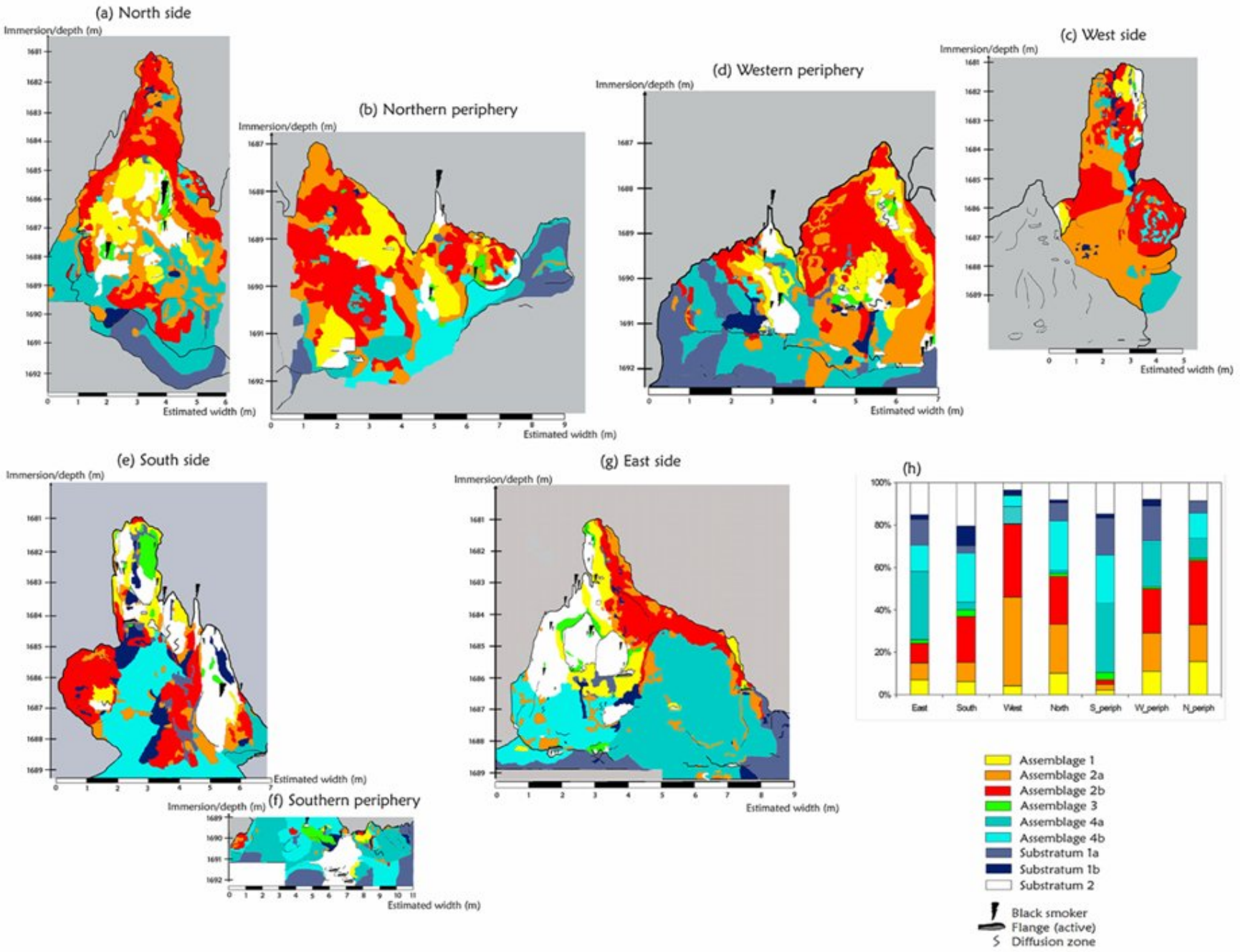
(a) North side
Immersion/depth (m)
Estimated width (m)
(b) Northern periphery
Immersion/depth (m)
Estimated width (m)
(c) West side
Immersion/depth (m)
Estimated width (m)
(d) Western periphery
Immersion/depth (m)
Estimated width (m)
(e) South side
Immersion/depth (m)
Estimated width (m)
(f) Southern periphery
Immersion/depth (m)
Estimated width (m)
(g) East side
Immersion/depth (m)
Estimated width (m)
(h)
100%
80%
60%
40%
20%
0%
East
South
West
North
S_periph
W_periph
N_periph
Assemblage 1
Assemblage 2a
Assemblage 2b
Assemblage 3
Assemblage 4a
Assemblage 4b
Substratum 1a
Substratum 1b
Substratum 2
Black smoker
Flange (active)
Diffusion zone

Fig. 3.

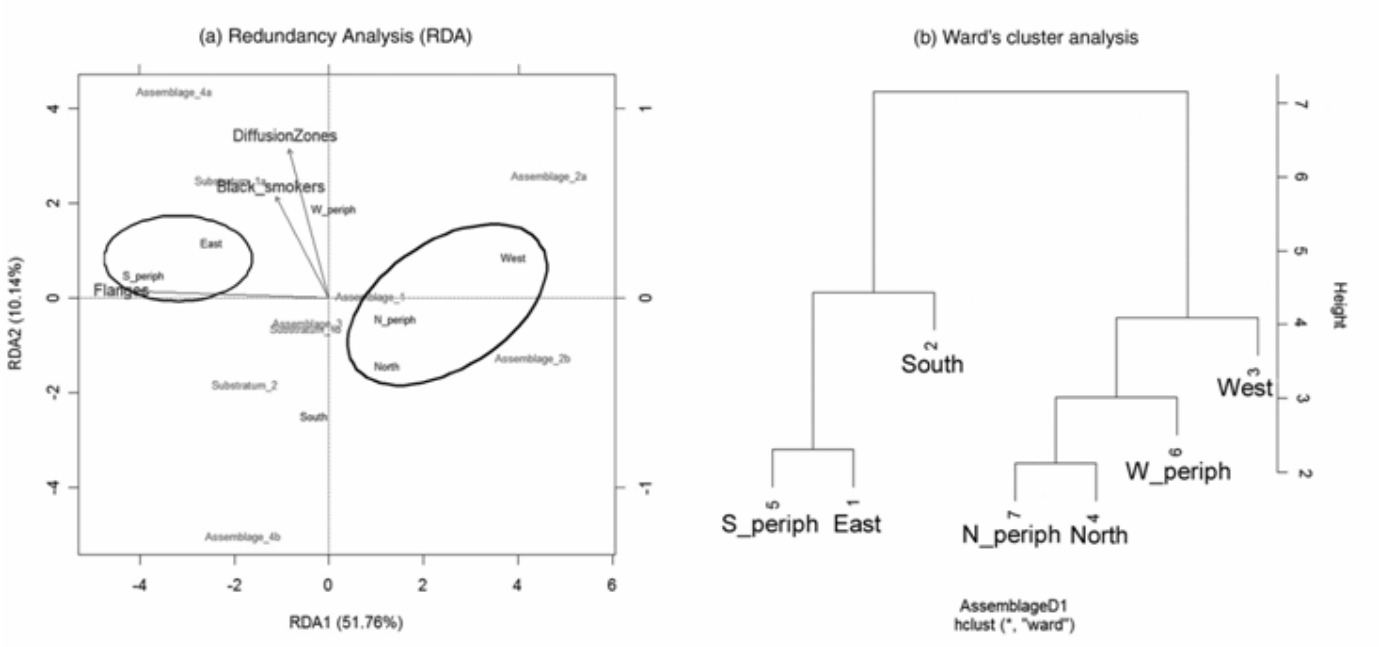

Fig. 4.

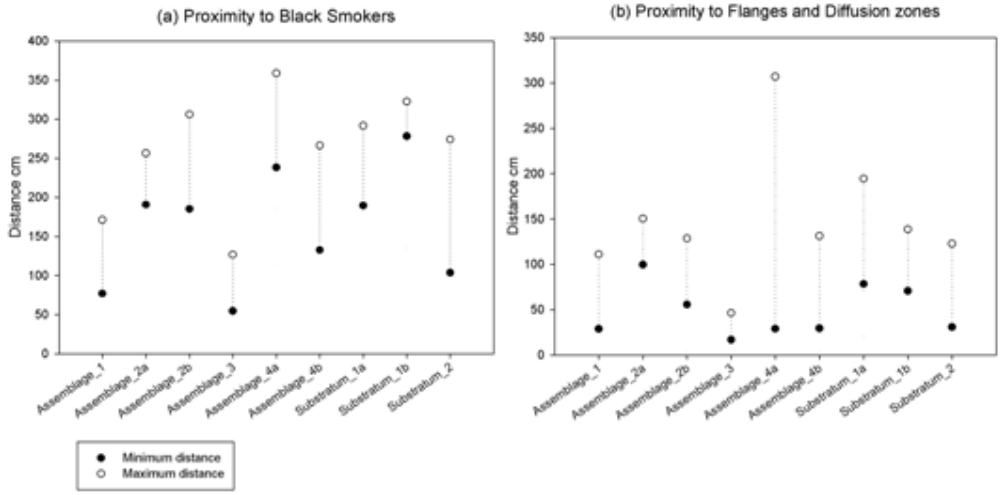

Fig. 5.

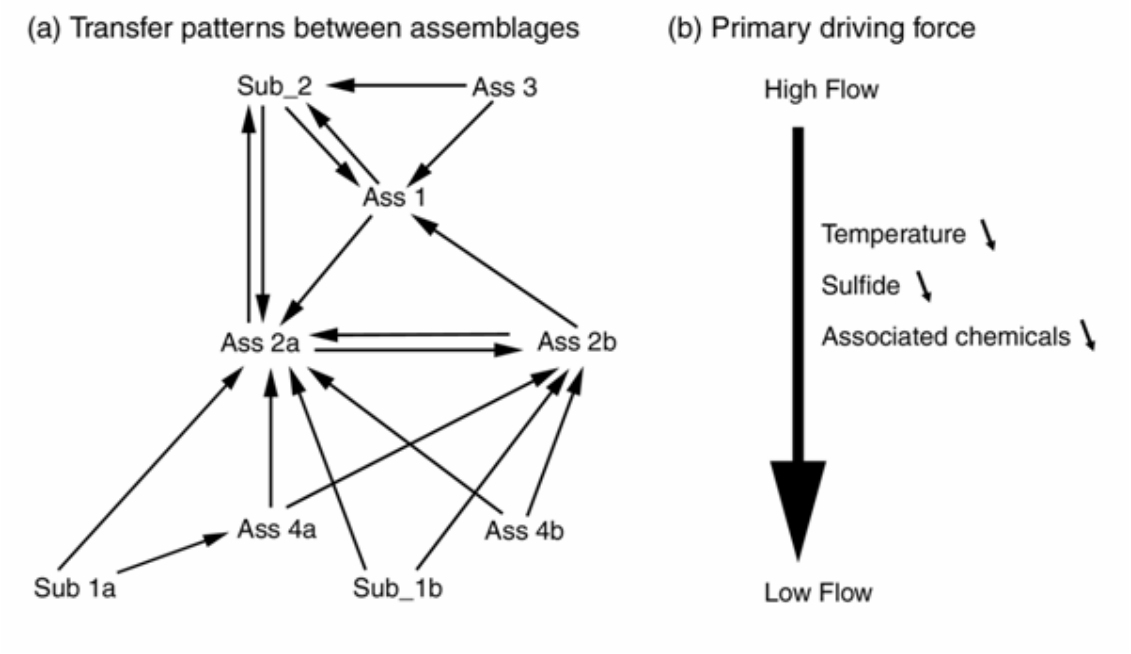
(a) Transfer patterns between assemblages
(b) Primary driving force
Sub_2
Ass 3
Ass 1
Ass 2a
Ass 2b
Ass 4a
Ass 4b
Sub 1a
Sub_1b
High Flow
Temperature
Sulfide
Associated chemicals
Low Flow

Fig. 6.

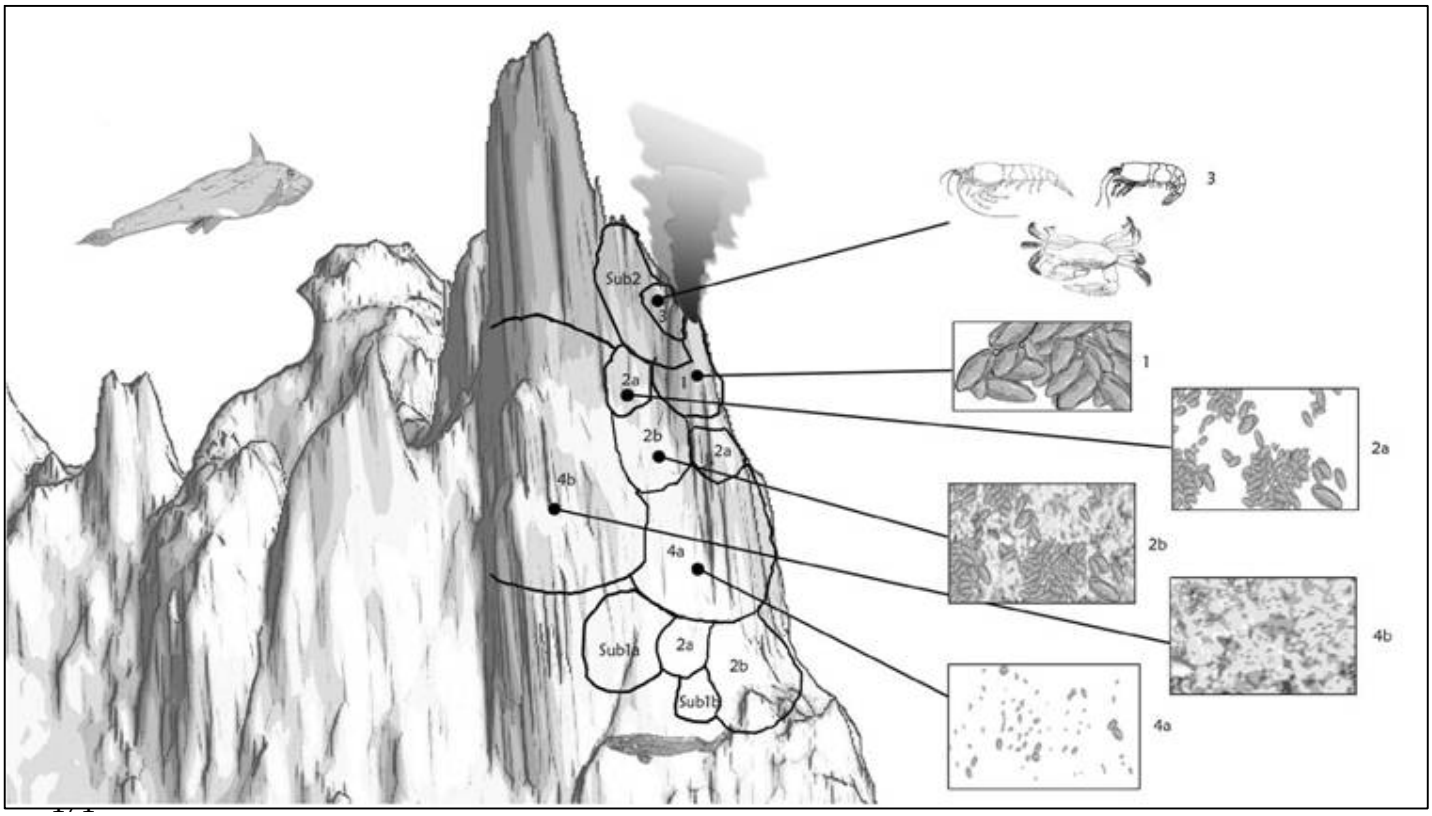
Sub2
2a
1
2b
2a
4b
4a
Sub1a
2a
2b
Sub1b
3
1
2a
2b
4b
4a

Fig. 7.